A Space-Time Finite Element Method for the Exterior Structural Acoustics Problem: Time-Dependent Radiation Boundary Conditions in Two Space Dimensions

by

Lonny L. Thompson

Department of Mechanical Engineering
Clemson University
Clemson, South Carolina 29634-0921

July 1995

Abstract

A time-discontinuous Galerkin space-time finite element method is formulated for the exterior structural acoustics problem in two space dimensions. The problem is posed over a bounded computational domain with local time-dependent radiation (absorbing) boundary conditions applied to the fluid truncation boundary. Aborbing boundary conditions are incorporated as 'natural' boundary conditions in the space-time variational equation, i.e. they are enforced weakly in both space and time. Following Bayliss and Turkel, time-dependent radiation boundary conditions for the two-dimensional wave equation are developed from an asymptotic approximation to the exact solution in the frequency domain expressed in negative powers of a nondimensional wavenumber. In this paper we undertake a brief development of the time-dependent radiation boundary conditions, establishing their relationship to the exact impedance (DtN map) for the acoustic fluid, and characterize their accuracy when implemented in our space-time finite element formulation for transient structural acoustics. Stability estimates are reported together with an analysis of the positive form of the matrix problem emanating from the space-time variational equations for the coupled fluid-structure system. Several numerical simulations of transient radiation and scattering in two space dimensions are presented to demonstrate the effectiveness of the space-time method.

Contents

1 Introduction

A space-time finite element formulation is presented for solution of the exterior structural acoustics problem in two space dimensions involving the interaction of vibrating structures submerged in an infinite acoustic fluid and requiring solution of the coupled wave equation subject to a far-field radiation condition. The formulation is based on the time-discontinuous Galerkin finite element method developed by Hughes and Hulbert [1] for second-order hyperbolic equations. In this work, a space-time variational equation is presented for both the elastic structure and the acoustic fluid, together with their interaction. The method is especially useful for application of adaptive strategies for transient acoustics in which unstructured space-time meshes are used to track waves propagating along space-time characteristics. For exterior problems involving an infinite fluid domain, the formulation employs a finite computational fluid domain surrounding the structure and incorporates time-dependent non-reflecting (radiation) boundary conditions on the fluid truncation boundary as 'natural' boundary conditions in the space-time variational equation, i.e. they are enforced weakly in both space and time. For large-scale simulations the use of high-order accurate radiation boundary conditions is essential to allow the fluid truncation boundary to be placed close to the structure and thereby minimizing the mesh and matrix problem size.

High-order accurate radiation boundary conditions have been proposed by several authors; complete surveys prior to 1991 can be found in Givoli [2] and Abboud [3]. In the work presented in [4, 5, 6] a general framework has been established for the incorporation of high-order accurate boundary conditions in the time-discontinuous Galerkin space-time finite element method. In Thompson and Pinsky [6, 7] details for the development and implementation of high-order accurate non-reflecting boundary conditions for solutions of the scalar wave equation in three space dimensions are given. In particular, a new sequence of exact radiation boundary conditions which are in the form of local (differential) operators in time were derived and incorporated into the time-discontinuous Galerkin variational equations. These high-order accurate non-reflecting boundary conditions are based on the exact impedance relation for the acoustic fluid expressed through the Dirichlet-to-Neumann (DtN) map in the frequency domain [8], and are exact for solutions consisting of the first N spherical wave harmonics in three dimensions. The development of these boundary conditions makes use of the special property that the high-order spherical Hankel functions appearing in the impedance coefficients of the three-dimensional DtN map can be expressed in terms of the zero-order spherical Hankel function multiplied by a finite series in powers of a nondimensional wavenumber. As a consequence of this special form of the impedance coefficients, an exact inverse Fourier transform can be obtained yielding time-dependent counterparts that are exact for the first N spherical wave harmonics in both time and space.

In contrast, for the wave equation in two spatial dimensions it is not possible to express high-order cylindrical (integer) Hankel functions appearing in the exact DtN impedance relation solely in terms of the zero-order cylindrical Hankel function. As a consequence, in the two-dimensional case it is not possible to obtain local time-dependent radiation boundary conditions that exactly represent outgoing cylindrical wave harmonics. The difference between the two dimensional and three dimensional cases can be interpreted physically by the difference in the fundamental solution to the wave equation in two and three dimensions. In the three dimensional case, waves propagate along space-time characteristics with constant phase and can be represented exactly by local (differential) operators in time. In the two-dimensional case fundamental solutions propagate with a trailing wake behind the wave front creating a time history that cannot be exactly represented by simple local operators in time.

While it is possible to obtain spatially local non-reflecting boundary conditions in the frequency domain that exactly represent the first N cylindrical wave harmonics, (see Givoli and Keller [9]), exact time-dependent counterparts are not readily obtained due to the difficulty in obtaining an exact inverse Fourier transform for the two-dimensional Hankel function. By taking advantage of an asymptotic approximation for the two-dimensional Hankel function for large values of a non-dimensional wavenumber kR, where R is the radial distance to the fluid truncation boundary, an approximate localization of the exact impedance relation, i.e. the Dirichlet-to-Neumann map, can be obtained which has a direct time-dependent counterpart through application of an inverse Fourier transform.

The localization proceeds by first recasting the exact solution for the exterior problem as a power series expansion in terms of the zero-order and first-order cylindrical Hankel functions. By using a far-field approximation for large kR, an asymptotic expansion is constructed in terms of negative powers of the wavenumber and the radial distance to the artificial boundary. Following the procedure outlined in Bayliss and Turkel [10, 11], a sequence of local (differential) operators are then derived which satisfy the first m terms in this asymptotic expansion. This can be considered as a way of matching the first m terms of an approximate solution for outgoing waves on the radiation boundary. The operators in this sequence are of progressively higher order and provide increasing accuracy as more terms are matched in the expansion. An important property of these approximate boundary operators is that they have an exact inverse Fourier transform allowing a family of boundary conditions to be defined which are local in space and time.

In this paper we undertake a brief development of the time-dependent radiation boundary conditions for two-dimensional wave propagation, establishing their relationship to the exact impedance (DtN map) for the acoustic fluid, and characterize their accuracy when implemented in our space-time finite element formulation for transient structural acoustics. In addition, stability estimates are reported together with an analysis of the positive form of the matrix problem emanating from the space-time variational equations for the coupled fluid-structure system. Crucial to the unconditional stability and optimal convergence rates of the formulation is the introduction of consistent temporal jump operators across space-time slabs restricted to the radiation boundary. The specific form of these operators are designed such that continuity of the solution across slabs is weakly enforced in a form consistent with the two-dimensional absorbing boundary conditions. Direct implementation of these radiation boundary conditions in a semidiscrete Galerkin finite element formulation have been previously reported in [12, 13].

An overview of the paper is as follows: In Section 2 the coupled system for the exterior fluid-structure interaction problem is described together with a statement of the strong (local) form of the initial/boundary-value problem of structural acoustics. An important feature in the development is the choice of scalar velocity potential for the acoustic fluid in conjunction with the displacement vector for the structure as the fundamental variables for the coupled system. As a consequence of this choice of variables the space-time formulation for structural acoustics is unconditionally stable and converges at an optimal rate in a norm which is stronger than the total energy norm for the system. In Section 3 the reader is introduced to the fundamental concepts of space-time finite element technology where the space-time domain is partitioned into a sequence of space-time slabs. In Section 3.1 the space-time variational equations incorporating a first-order accurate non-reflecting boundary condition in two space dimensions are described. In Section 3.2 details are given for the assembly and form of the space-time matrix equations emanating from the variational equation for the coupled fluid/structure system including non-reflecting boundary conditions. Stability estimates are reported together with an analysis of the positive form of the matrix problem for structural acoustics. In Section 4 the development of high-order accurate non-reflecting boundary conditions for the wave equation in two space dimensions is discussed. The development begins with the exact DtN map in the frequency domain followed by a localization and inverse Fourier transform procedure to obtain local boundary conditions in the time domain. This section concludes with details for the

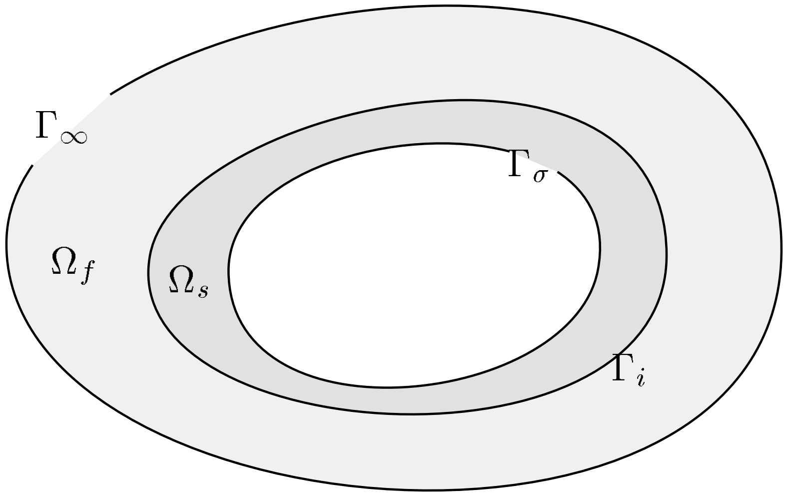

Fig. 1. Coupled system for the exterior fluid-structure interaction problem, with artificial boundary Γ_∞ enclosing the finite computational domain $\Omega = \Omega_f \cup \Omega_s$.

implementation of these high-order time-dependent radiation boundary conditions in the space-time variational formulation. Finally, in Section 5 numerical examples are presented.

2 The Transient Structural Acoustics Problem

The coupled fluid-structure system is illustrated in Figure 1, and consists of the artificial truncation boundary Γ_∞ enclosing the finite computational domain Ω. The finite computational domain is composed of the fluid domain Ω_f, which in turn surrounds the structural domain Ω_s such that $\Omega = \Omega_f \cup \Omega_s$. The fluid boundary $\partial\Omega_f$, is divided into the fluid-structure interface boundary Γ_i, and the artificial boundary Γ_∞. The structural boundary $\partial\Omega_s$, is composed of the shared fluid-structure interface boundary Γ_i and a traction boundary Γ_σ. The infinite domain outside the artificial boundary is denoted by Ω_∞. The temporal interval of interest is $I =]0, T[$ and the number of spatial dimensions is n_{sd}. In this paper we concentrate on the two-dimensional problem where $n_{sd} = 2$.

The governing equations for the structure are stated for a linear solid continuum. The acoustic fluid is modeled under the usual assumptions governing sound wave propagation; a compressible and inviscid fluid linearized about an equilibrium state with constant density and velocity.

2.1 The Strong Form

The strong (local) form of the fluid-structure initial/boundary-value problem may be stated as:

Given a prescribed traction $\bar{\boldsymbol{t}} : \Gamma_\sigma \times I \mapsto \mathbb{R}^{n_{sd}}$ and a source $f : \Omega_f \times I \mapsto \mathbb{R}$,
Find $\boldsymbol{u} : \bar{\Omega}_s \times I \mapsto \mathbb{R}^{n_{sd}}$, and $\phi : \bar{\Omega}_f \times I \mapsto \mathbb{R}$, such that

$$\nabla \cdot \boldsymbol{\sigma} = \rho_s \ddot{\boldsymbol{u}} \qquad \text{in } \; Q_s := \Omega_s \times I \tag{1}$$

$$\boldsymbol{\sigma} = \boldsymbol{C} : \nabla^s \boldsymbol{u} \qquad \text{in } \; Q_s := \Omega_s \times I \tag{2}$$

$$\nabla^2 \phi - a^2 \ddot{\phi} = f \qquad \text{in } \; Q_f := \Omega_f \times I \tag{3}$$

$$\boldsymbol{\sigma} \cdot \boldsymbol{n} = \bar{\boldsymbol{t}} \qquad \text{on } \; \Upsilon_\sigma := \Gamma_\sigma \times I \tag{4}$$

$$\boldsymbol{\sigma} \cdot \boldsymbol{n} = \rho_0 \dot{\phi} \boldsymbol{n} \qquad \text{on } \; \Upsilon_i := \Gamma_i \times I \tag{5}$$

$$\nabla \phi \cdot \boldsymbol{n} = \dot{\boldsymbol{u}} \cdot \boldsymbol{n} \qquad \text{on } \; \Upsilon_i := \Gamma_i \times I \tag{6}$$

$$\nabla \phi \cdot \boldsymbol{n} = -\mathbb{S}_m \phi \qquad \text{on } \; \Upsilon_\infty := \Gamma_\infty \times I \tag{7}$$

In the above, $\boldsymbol{u}(\boldsymbol{x}, t)$ with $\boldsymbol{x} \in \Omega_s$, is the structural displacement vector, $\boldsymbol{\sigma}$ is the symmetric Cauchy stress tensor, and $\phi(\boldsymbol{x}, t)$ with $\boldsymbol{x} \in \Omega_f$, is the scalar velocity potential for the irrotational acoustic fluid. We denote the phase velocity of acoustic wave propagation by $c > 0$, with slowness $a = c^{-1}$ and $\rho_s > 0$ and $\rho_0 > 0$ are the reference densities of the structure and fluid respectively. The acoustic source loading is given by f and the prescribed traction on the structure is $\bar{\boldsymbol{t}}$, where $\boldsymbol{n}$ is the unit outward normal to Ω_s, and inward normal to Ω_f on Γ_i, and outward normal to Ω_f on Γ_∞. A superposed dot indicates partial differentiation with respect to t, and ∇^s refers to the symmetric gradient. The acoustic pressure p, and the acoustic velocity $\boldsymbol{v}$, are related to the velocity potential by $p = -\rho_0 \dot{\phi}$ and $\boldsymbol{v} = \nabla \phi$.

As a consequence of the above coupled second-order system of hyperbolic equations, we have the initial conditions,

$$\boldsymbol{u}(\boldsymbol{x}, 0) = \boldsymbol{u}_0(\boldsymbol{x}) \; ; \qquad \dot{\boldsymbol{u}}(\boldsymbol{x}, 0) = \dot{\boldsymbol{u}}_0(\boldsymbol{x}) \qquad \boldsymbol{x} \in \Omega_s \tag{8}$$

$$\phi(\boldsymbol{x}, 0) = \phi_0(\boldsymbol{x}) \; ; \qquad \dot{\phi}(\boldsymbol{x}, 0) = \dot{\phi}_0(\boldsymbol{x}) \qquad \boldsymbol{x} \in \Omega_f \tag{9}$$

Equation (1) governs the linear momentum balance of the structure, while (2) is the constitutive relationship written here for linear elasticity. Equation (3) is the acoustic scalar wave equation, Equation (6) is the normal velocity compatibility condition across the fluid-structure interface, and (5) represents the fluid pressure acting on the structure. Equation (4) is the applied traction. Equation (7) represents the radiation boundary condition imposed on the artificial boundary Γ_∞ which approximates the asymptotic behavior of the solution at infinity, as described by the Sommerfeld radiation condition:

$$\lim_{r\to\infty} r^{1/2}\left(\frac{\partial}{\partial r}+\frac{1}{c}\frac{\partial}{\partial t}\right)\phi = 0 \qquad r+ct=\text{constant} \tag{10}$$

where r is the radial distance from the source. This condition asserts that at infinity all waves are outgoing. The boundary condition (7) can take several different forms depending on the local (differential) or nonlocal (integral) operators appearing in the definition of the linear map $\mathbb{S}_m$.

For Γ_∞ taken to be a circle in two spatial dimensions $\mathbb{R}^2$, the obvious choice for $\mathbb{S}_m$ is to use a simple Sommerfeld-like boundary condition of the form,

$$\nabla\phi\cdot\boldsymbol{n} \quad = \quad -\frac{1}{c}\dot{\phi} \qquad \text{on} \quad \Upsilon_\infty := \Gamma_\infty\times]0,T[\tag{11}$$

where $\nabla\phi\cdot\boldsymbol{n} = \partial\phi/\partial n$ is the normal derivative on Γ_∞. Restated in terms of pressure, $p=-\rho_0\dot{\phi}$, and velocity $\boldsymbol{v}=\nabla\phi$, equation (11) becomes $\boldsymbol{v}\cdot\boldsymbol{n} = p/z_o$, where $z_o=\rho_0 c$, is the characteristic impedance for plane-wave propagation. This boundary condition is exact in one-dimension for any position, however in multi-dimensions, when (11) is applied at a finite distance from the source of excitation, this boundary condition will generally produce large spurious reflections, resulting in unacceptable errors in the numerical solution. Because of the potential loss of accuracy resulting from the use of (11), an improved non-reflecting boundary is needed. A number of high-order accurate non-reflecting boundary conditions which take the form of (7) are available and will be discussed further in Section 4. Here we note that the index m, is related to the order of temporal derivatives appearing in the operator. An example is the first-order boundary condition,

$$\frac{\partial\phi}{\partial n} = -\mathbb{S}_1\phi, \qquad \text{where} \quad \mathbb{S}_1 := \frac{1}{2R}+\frac{1}{c}\frac{\partial}{\partial t} \tag{12}$$

where R is the radial distance to a circular boundary Γ_∞. This radiation boundary condition is referred to as a 'cylindrical damper' since at the asymptotic limit of large frequencies, this operator completely absorbs radially symmetric cylindrical waves.

3 A Space-Time FEM for Structural Acoustics

The development of the space-time finite element method (FEM) proceeds by considering an ordered partition of the time interval, $I=]0,T[$, of the form: $0=t_0<$

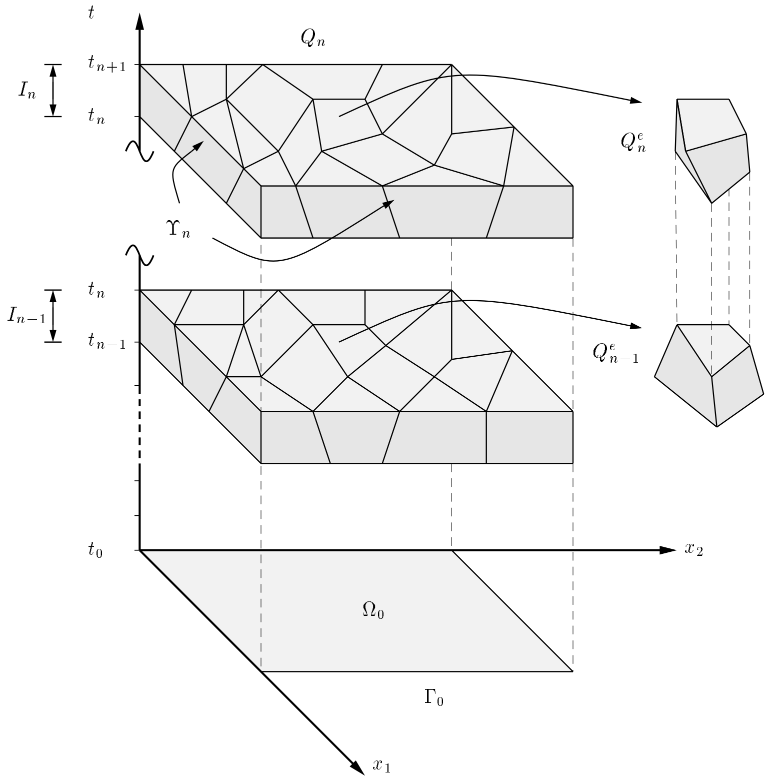

Fig. 2. Illustration of two consecutive space-time slabs with unstructured finite element meshes in space-time.

$t_1 < \ldots < t_N = T$ where the nth time interval is denoted, $I_n :=]t_n, t_{n+1}[$. Using this notation the nth space-time slab for the structure and fluid are respectively,

$$Q_n^s = \Omega_s \times I_n \qquad , \qquad Q_n^f = \Omega_f \times I_n \tag{13}$$

with boundaries $\Upsilon_n^s = \partial\Omega_s \times I_n$ and $\Upsilon_n^f = \partial\Omega_f \times I_n$.

Figure 2 shows an illustration of two consecutive space-time slabs Q_{n-1} and Q_n for the fluid where the superscript is omitted for clarity. Within each space-time element, the trial solution and weighting function are approximated by pth-order polynomials in $\boldsymbol{x}$ and t. These functions are assumed $C^0(Q_n)$ continuous throughout each space-time slab, but are allowed to be discontinuous across the interfaces of the slabs. The trial functions are defined by the following spaces:

Trial structural displacements

$$\mathcal{S}^h = \bigcup_{n=0}^{N-1} \mathcal{S}_n^h, \qquad \mathcal{S}_n^h = \left\{ \boldsymbol{u}^h(\boldsymbol{x},t) \middle| \boldsymbol{u}^h \in (C^0(Q_n^s))^{n_{sd}}, \, \boldsymbol{u}^h\Big|_{Q_n^{s^e}} \in (\mathcal{P}^p(Q_n^{s^e}))^{n_{sd}} \right\}$$

Trial fluid potential

$$\mathcal{T}^h = \bigcup_{n=0}^{N-1} \mathcal{T}_n^h, \qquad \mathcal{T}_n^h \quad = \quad \left\{ \phi^h(\boldsymbol{x},t) \middle| \phi^h \in C^0(Q_n^f), \, \phi^h\Big|_{Q_n^{f^e}} \in \mathcal{P}^p(Q_n^{f^e}) \right\}$$

where $\mathcal{P}^p$ denotes the space of pth-order polynomials within a space-time element Q_n^e. Assuming the function $\phi^h(\boldsymbol{x}\,,\,t)$ to be discontinuous at time t_n, suppressing the argument $\boldsymbol{x}$, the temporal jump operator is defined by,

$$[\![\phi^h(t_n)]\!] := \phi^h(t_n^+) \;-\; \phi^h(t_n^-) \tag{14}$$

where

$$\phi^h(t_n^\pm) = \lim_{\epsilon\to 0\pm} \phi^h(t_n+\epsilon)$$

This discontinuity of the finite element functions across space-time slab interfaces, allows for the general use of hierarchical and spectral-type interpolations in both space and time, and provides freedom of changing the spatial discretization from one time step to another. The jump operators are essential for establishing the unconditional stability and positive form of the matrix equations of the Discontinuous Galerkin space-time FEM.

Before stating the space-time variational equations, the following bilinear operators are defined:

$$(\boldsymbol{w}^h\,,\,\boldsymbol{u}^h)_{\Omega_s} \;=\; \int_{\Omega_s} \boldsymbol{w}^h\cdot\boldsymbol{u}^h\,d\Omega \tag{15}$$

$$a(\boldsymbol{w}^h\,,\,\boldsymbol{u}^h)_{\Omega_s} \;=\; \int_{\Omega_s} \nabla\boldsymbol{w}^h\cdot\boldsymbol{\sigma}(\nabla\boldsymbol{u}^h)\,d\Omega \tag{16}$$

$$(w^h\,,\,\phi^h)_{\Omega_f} \;=\; \int_{\Omega_f} \rho_0\,w^h\,\phi^h\,d\Omega \tag{17}$$

$$(w^h\,,\,\phi^h)_{Q_n^f} \;=\; \int_{t_n}^{t_{n+1}} (w^h\,,\,\phi^h)_{\Omega_f}\,dt \tag{18}$$

$$(w^h\,,\,\phi^h)_{(\Upsilon_\infty)_n} \;=\; \int_{t_n}^{t_{n+1}} (w^h\,,\,\phi^h)_{\Gamma_\infty}\,dt \tag{19}$$

Note that inner products for the fluid are weighted by the fluid reference density ρ_0. The meaning of other similar notations may be inferred from these.

3.1 Time-Discontinuous Galerkin Formulation

The space-time variational formulation for the exterior transient structural acoustics problem is obtained from a weighted residual of the governing equations (1)–(7) within a space-time slab and incorporates time-discontinuous jump terms across slab interfaces. The time-discontinuous method is applied in one space-time slab at a time; data from the end of the previous slab are employed as initial conditions for the current slab. For simplicity the variational equations are stated for the first-order radiation boundary conditions defined in (12). Extensions to higher-order radiation boundary conditions are given in Section 4.

3.1.1 Space-Time Variational Equations

Within each space-time slab, $n = 0, 1, \ldots, N-1$, the object is to find $\{\boldsymbol{u}^h, \phi^h\} \in \mathcal{S}_n^h \times \mathcal{T}_n^h$, such that for all weighting functions $\{\boldsymbol{w}^h, w^h\} \in \mathcal{S}_n^h \times \mathcal{T}_n^h$, the following coupled variational equations are satisfied,

$$\begin{aligned} E_s(\boldsymbol{w}^h, \boldsymbol{u}^h)_n - A(\boldsymbol{w}^h, \phi^h)_n &= L_s(\boldsymbol{w}^h)_n && (20)\\ E_f(w^h, \phi^h)_n + E_r(w^h, \phi^h)_n + A(\boldsymbol{u}^h, w^h)_n &= L_f(w^h)_n + L_r(w^h)_n && (21) \end{aligned}$$

with the following definitions,

$$\begin{aligned} E_s(\boldsymbol{w}^h, \boldsymbol{u}^h)_n &:= (\dot{\boldsymbol{w}}^h, \rho_s \ddot{\boldsymbol{u}}^h)_{Q_n^s} + a(\dot{\boldsymbol{w}}^h, \boldsymbol{u}^h)_{Q_n^s} \\ &\quad + (\dot{\boldsymbol{w}}^h(t_n^+), \rho_s \dot{\boldsymbol{u}}^h(t_n^+))_{\Omega_s} + a(\boldsymbol{w}^h(t_n^+), \boldsymbol{u}^h(t_n^+))_{\Omega_s} && (22)\\ E_f(w^h, \phi^h)_n &:= (\dot{w}^h, a^2 \ddot{\phi}^h)_{Q_n^f} + (\nabla \dot{w}^h, \nabla \phi^h)_{Q_n^f} \\ &\quad + (\dot{w}^h(t_n^+), a^2 \dot{\phi}^h(t_n^+))_{\Omega_f} + (\nabla w^h(t_n^+), \nabla \phi^h(t_n^+))_{\Omega_f} && (23)\\ E_r(w^h, \phi^h)_n &:= \frac{1}{2R}(\dot{w}^h, \phi^h)_{(\Upsilon_\infty)_n} + \frac{1}{c}(\dot{w}^h, \dot{\phi}^h)_{(\Upsilon_\infty)_n} \\ &\quad + \frac{1}{2R}(w^h(t_n^+), \phi^h(t_n^+))_{\Gamma_\infty} && (24)\\ A(\boldsymbol{w}^h, \phi^h)_n &:= (\dot{\boldsymbol{w}}^h, \rho_0 \dot{\phi}^h \boldsymbol{n})_{(\Upsilon_i)_n} && (25) \end{aligned}$$

and loading operators,

$$\begin{aligned} L_s(\boldsymbol{w}^h)_n &:= (\dot{\boldsymbol{w}}^h, \bar{\boldsymbol{t}})_{(\Upsilon_\sigma)_n} \\ &\quad + (\dot{\boldsymbol{w}}^h(t_n^+), \rho_s \dot{\boldsymbol{u}}^h(t_n^-))_{\Omega_s} + a(\boldsymbol{w}^h(t_n^+), \boldsymbol{u}^h(t_n^-))_{\Omega_s} && (26)\\ L_f(w^h)_n &:= (\dot{w}^h, f)_{Q_n^f} \\ &\quad + (\dot{w}^h(t_n^+), a^2 \dot{\phi}^h(t_n^-))_{\Omega_f} + (\nabla w^h(t_n^+), \nabla \phi^h(t_n^-))_{\Omega_f} && (27)\\ L_r(w^h)_n &:= \frac{1}{2R}(w^h(t_n^+), \phi^h(t_n^-))_{\Gamma_\infty} && (28) \end{aligned}$$

The initial data at $n = 0$ is given by the initial conditions $\boldsymbol{u}^h(t_0^-) = \boldsymbol{u}_0$ and $\dot{\boldsymbol{u}}^h(t_0^-) = \dot{\boldsymbol{u}}_0$, together with $\phi^h(t_0^-) = \phi_0$ and $\dot{\phi}^h(t_0^-) = \dot{\phi}_0$.

In the operator $E_s(\boldsymbol{w}^h, \boldsymbol{u}^h)_n$, the terms evaluated over Q_n^s, act to weakly enforce the momentum balance in the structure while in $E_f(w^h, \phi^h)_n$, the terms evaluated over Q_n^f, act to weakly enforce the scalar wave equation in the fluid within the interior of the nth space-time slab. The definition of the radiation boundary operator

$E_r(w^h\,,\,\phi^h)_n$, is stated here for the first-order radiation boundary condition $\mathbb{S}_1$ defined earlier in (12). The radiation boundary conditions are incorporated as natural boundary conditions in the variational equation, i.e., they are enforced weakly through integration over both the artificial boundary Γ_∞ and the time interval I_n.

The coupling between the structure and fluid occurs through the operators $A(\cdot\,,\,\cdot)_n$ integrated over the fluid-structure interface $(\Upsilon_i)_n = \Gamma_i \times I_n$. These coupling terms appearing in (20) and (21) weakly enforce the acoustic pressure interface condition (5) and continuity of normal velocity condition (6) across the fluid-structure interface.

The jump terms evaluated over Ω_s in (22) and (26) act to weakly enforce continuity of the structural displacements across space-time slab interfaces. Similarly, the jump terms evaluated over Ω_f in (23) and (27) together with the terms evaluated over Γ_∞ in (24) and (28) act to weakly enforce continuity of the acoustic velocity potential across space-time slab interfaces. Because the solution is weakly enforced across slab interfaces, the finite element mesh may change from one slab to the next. This is especially useful in self-adaptive schemes where the finite element discretization can be enriched within space-time slabs to track wave fronts as they propagate along space-time characteristics.

For additional stability and to aid in the proof of convergence, least-squares operators based on local residuals of the Euler-Lagrange equations for the coupled system, including time-dependent radiation boundary conditions, can be incorporated into (20) and (21); see [5, 6]. Stabilized methods of this type are referred to as Galerkin Least Squares (GLS) methods [14] and provide additional stability and control of the residual of the finite element solution without degrading the accuracy of the underlying time-discontinuous Galerkin method.

3.2 Space-Time Matrix Equations

Matrix equations are constructed in an element-by-element fashion via standard finite element assembly algorithms. Representing shape functions locally at the element level by the function $N_a^e(\boldsymbol{x}\,,\,t)$, where $a = 1, 2, \cdots n_{en}$ is the local node number within element Q_n^e, and arranging in vector form as $\boldsymbol{N}^e(\boldsymbol{x}\,,\,t) = [N_1^e\,,\,N_2^e\,,\,\cdots\,,\,N_{n_{en}}^e]$, the space-time approximations can be written as,

$$\boldsymbol{u}^h(\boldsymbol{x},t) = \boldsymbol{N}_s^e(\boldsymbol{x},t)\,\boldsymbol{d}^e, \qquad (\boldsymbol{x},t) \in Q_n^{s^e} \tag{29}$$

$$\phi^h(\boldsymbol{x},t) = \boldsymbol{N}_f^e(\boldsymbol{x},t)\,\phi^e, \qquad (\boldsymbol{x},t) \in Q_n^{f^e} \tag{30}$$

where $\boldsymbol{N}_s^e(\boldsymbol{x},t)$ and $\boldsymbol{N}_f^e(\boldsymbol{x},t)$ are the e^{th} element shape function vectors for the structure and fluid respectively, and $\boldsymbol{d}^e$ and ϕ^e are the element structure displacement and fluid velocity potential solution vectors. Global solution vectors $\boldsymbol{d}$ and $\boldsymbol{\phi}$ may be stated in terms of local element solution vectors using the relations,

$$\boldsymbol{d}^e = \boldsymbol{A}_s^e \boldsymbol{d}, \qquad \boldsymbol{\phi}^e = \boldsymbol{A}_f^e \boldsymbol{\phi}$$

where $\boldsymbol{A}_s^e$ and $\boldsymbol{A}_f^e$ are boolean matrices. Substituting (29) and (30) along with corresponding approximations for the weighting functions into the space-time variational equations (20) and (21), yields for each space-time slab, $n = 0, 1, \cdots, N-1$, the following coupled system of matrix equations:

$$\begin{bmatrix} \boldsymbol{K}_s & -\boldsymbol{A} \\ \boldsymbol{A}^T & \boldsymbol{K}_f + \boldsymbol{K}_r \end{bmatrix} \begin{Bmatrix} \boldsymbol{d} \\ \boldsymbol{\phi} \end{Bmatrix} = \begin{Bmatrix} \boldsymbol{F}_s \\ \boldsymbol{F}_f + \boldsymbol{F}_r \end{Bmatrix} \tag{31}$$

The global matrices emanating from (23),(24) and (27),(28) are given by,

$$\boldsymbol{K}_f = \sum_{e=1}^{(n_{el})_n^f} \boldsymbol{A}_f^{e^T} \boldsymbol{k}_f^e \boldsymbol{A}_f^e, \qquad \boldsymbol{F}_f = \sum_{e=1}^{(n_{el})_n^f} \boldsymbol{A}_f^{e^T} \boldsymbol{f}_f^e \tag{32}$$

$$\boldsymbol{K}_r = \sum_{e=1}^{(n_{el})_n^f} \boldsymbol{A}_f^{e^T} \boldsymbol{k}_r^e \boldsymbol{A}_f^e, \qquad \boldsymbol{F}_r = \sum_{e=1}^{(n_{el})_n^f} \boldsymbol{A}_f^{e^T} \boldsymbol{f}_r^e \tag{33}$$

where

$$\begin{aligned} \boldsymbol{k}_f^e &= \int_{t_n}^{t_{n+1}} \int_{\Omega_f^e} \left(\frac{\rho_0}{c^2} (\boldsymbol{N}_{f,t}^e)^T \boldsymbol{N}_{f,tt}^e + \rho_0 (\nabla \boldsymbol{N}_{f,t}^e)^T \nabla \boldsymbol{N}_f^e \right) d\Omega \, dt \\ &+ \int_{\Omega_f^e} \left(\frac{\rho_0}{c^2} (\boldsymbol{N}_{f,t}^e(t_n^+))^T \boldsymbol{N}_{f,t}^e(t_n^+) + \rho_0 (\nabla \boldsymbol{N}_f^e(t_n^+))^T \nabla \boldsymbol{N}_f^e(t_n^+) \right) d\Omega \end{aligned} \tag{34}$$

$$\begin{aligned} \boldsymbol{k}_r^e &= \int_{t_n}^{t_{n+1}} \int_{\Gamma_\infty^e} \left(\frac{\rho_0}{2R} (\boldsymbol{N}_{f,t}^e)^T \boldsymbol{N}_f^e + \frac{\rho_0}{c} (\boldsymbol{N}_{f,t}^e)^T \boldsymbol{N}_{f,t}^e \right) d\Gamma \, dt \\ &+ \int_{\Gamma_\infty^e} \frac{\rho_0}{2R} (\boldsymbol{N}_f^e(t_n^+))^T \boldsymbol{N}_f^e(t_n^+) d\Gamma \end{aligned} \tag{35}$$

and

$$\begin{aligned} \boldsymbol{f}_f^e &= \int_{t_n}^{t_{n+1}} \int_{\Omega_f^e} \rho_0 (\boldsymbol{N}_{f,t}^e)^T f(t) d\Omega \, dt \\ &+ \int_{\Omega_f^e} \left(\frac{\rho_0}{c^2} (\boldsymbol{N}_{f,t}^e(t_n^+))^T \dot{\phi}^h(t_n^-) + \rho_0 (\nabla \boldsymbol{N}_f^e(t_n^+))^T \nabla \phi^h(t_n^-) \right) d\Omega \end{aligned} \tag{36}$$

$$\boldsymbol{f}_r^e = \int_{\Gamma_\infty^e} \frac{\rho_0}{2R} (\boldsymbol{N}_f^e(t_n^+))^T \phi^h(t_n^-) d\Gamma \tag{37}$$

In the above, $(n_{el})_n^f$ is the number of elements in the nth space-time domain Q_n^f. and the comma with subscript t on the finite element shape functions indicates the time derivative. Note that the weighting $w^h(\boldsymbol{x}\,,\,t_n^+)$ is evaluated using shape functions for the present space-time slab whereas the trial solution $\phi^h(\boldsymbol{x}\,,\,t_n^-)$ is evaluated with interpolations and nodal values of the previous slab. Expressions for structural arrays $\boldsymbol{K}_s$ and $\boldsymbol{F}_s$ are defined similarly, and can be deduced from (22) and (26). The matrix coupling the structural displacements to the fluid velocity potential emanates from (25) and is defined by,

$$\boldsymbol{A} \;=\; \sum_{e=1}^{(n_{el})_n} \boldsymbol{A}_s^{e^T} \int_{t_n}^{t_{n+1}} \int_{\Gamma_i^e} \rho_0 (\boldsymbol{N}_{s,t}^e)^T \, \boldsymbol{n}\, \boldsymbol{N}_{f,t}^e \, d\Gamma^e \, dt \boldsymbol{A}_f^e \tag{38}$$

As a consequence of choosing the velocity potential as the primary solution variable for the acoustic fluid, the system of algebraic equations (31) takes on a positive form. The positive form of (31) follows by considering the diagonal matrix partitions. For $\boldsymbol{K}_f$ we have,

$$\begin{aligned}
\boldsymbol{\phi}^T \boldsymbol{K}_f \boldsymbol{\phi} &= \sum_{e=1}^{(n_{el})_n^f} \boldsymbol{\phi}^T \boldsymbol{A}_f^{e^T} \boldsymbol{k}_f^e \boldsymbol{A}_f^e \boldsymbol{\phi} \\
&= \sum_{e=1}^{(n_{el})_n^f} \boldsymbol{\phi}^{e^T} \boldsymbol{k}_f^e \boldsymbol{\phi}^e \\
&= E_f(\phi^h\,,\,\phi^h)_n \\
&= \int_{t_n}^{t_{n+1}} \frac{\mathrm{d}}{\mathrm{d}t} \mathcal{E}_f(\phi^h(t))\, dt + 2\mathcal{E}_f(\phi^h(t_n^+)) \\
&= \mathcal{E}_f(\phi^h(t_{n+1}^-)) + \mathcal{E}_f(\phi^h(t_n^+)) \\
&\geq 0
\end{aligned} \tag{39}$$

In the above, the expression for the energy is defined as,

$$\mathcal{E}_f(\phi^h) \;=\; \frac{1}{2}\rho_0 \,||a\dot{\phi}^h||_{\Omega_f}^2 \;+\; \frac{1}{2}\rho_0 \,||\nabla\phi^h||_{\Omega_f}^2 \tag{40}$$

and $||\cdot||_\Omega$ denotes the L_2 norm.

Similarly, for the matrix partition on the radiation boundary,

$$\boldsymbol{\phi}^T \boldsymbol{K}_r \boldsymbol{\phi} \;=\; E_r(\phi^h\,,\,\phi^h)_n \tag{41}$$

$$\begin{aligned}
&= \int_{t_n}^{t_{n+1}} \frac{1}{4R}\frac{\mathrm{d}}{\mathrm{d}t}(\phi^h(t)\,,\,\phi^h(t))_{\Gamma_\infty}\, dt + \int_{t_n}^{t_{n+1}} \frac{1}{c}(\dot{\phi}^h(t)\,,\,\dot{\phi}^h(t))_{\Gamma_\infty}\, dt \\
&+ \frac{1}{2R}(\phi^h(t_n^+)\,,\,\phi^h(t_n^+))_{\Gamma_\infty} \\
&= \frac{1}{4R}||\phi^h(t_{n+1}^-)||_{\Gamma_\infty}^2 + \frac{1}{4R}||\phi^h(t_n^+)||_{\Gamma_\infty}^2 + \frac{1}{c}\int_{t_n}^{t_{n+1}} ||\dot{\phi}^h(t)||_{\Gamma_\infty}^2\, dt \\
&\geq 0
\end{aligned} \tag{42}$$

Assuming that the elastic coefficients $\boldsymbol{C}$ defined in (2) satisfy pointwise stability, similar arguments can be used to show that the matrix partition $\boldsymbol{K}_s$ satisfies $\boldsymbol{d}^T\boldsymbol{K}_s\boldsymbol{d} \geq 0$. With these properties in hand, it follows that $\forall$ $\boldsymbol{d}$ and ϕ:

$$
\begin{aligned}
&\left\{ \begin{array}{c} \boldsymbol{d} \\ \phi \end{array} \right\}^T \left[\begin{array}{cc} \boldsymbol{K}_s & -\boldsymbol{A} \\ \boldsymbol{A}^T & \boldsymbol{K}_f + \boldsymbol{K}_r \end{array} \right] \left\{ \begin{array}{c} \boldsymbol{d} \\ \phi \end{array} \right\} \\
&= \boldsymbol{d}^T\boldsymbol{K}_s\boldsymbol{d} - \boldsymbol{d}^T\boldsymbol{A}\phi + \phi^T\boldsymbol{A}^T\boldsymbol{d} + \phi^T(\boldsymbol{K}_f + \boldsymbol{K}_r)\phi \\
&= \boldsymbol{d}^T\boldsymbol{K}_s\boldsymbol{d} + \phi^T(\boldsymbol{K}_f + \boldsymbol{K}_r)\phi \\
&\geq 0
\end{aligned} \tag{43}
$$

where we have used (39) and (42), and the property $\boldsymbol{d}^T\boldsymbol{A}\phi = \phi^T\boldsymbol{A}^T\boldsymbol{d}$.

The stability of the resulting algorithm follows directly from the positive form of the matrix equations. Using the result (43), it can be shown that in the absence of forcing terms, i.e., $\bar{\boldsymbol{t}} = \boldsymbol{0}$ and $f = 0$, and for $\mathbb{S}_1$, the total energy for the fluid-structure system,

$$
\mathbb{E}(\boldsymbol{u}\,,\,\phi) := \mathcal{E}_s(\boldsymbol{u}) + \mathcal{E}_f(\phi) \tag{44}
$$

plus the energy absorbed through the radiation boundary Γ_∞, is always less than, or equal to the initial energy in the system, i.e.,

$$
\begin{aligned}
&\mathcal{E}_s(\boldsymbol{u}^h(t_{n+1}^-)) + \mathcal{E}_f(\phi^h(t_{n+1}^-)) + \frac{1}{4R}||\phi^h(t_{n+1}^-)||^2_{\Gamma_\infty} + \frac{1}{c}\int_0^{t_{n+1}} ||\dot{\phi}^h(t)||^2_{\Gamma_\infty}\, dt \\
\leq\ &\mathcal{E}_s(\boldsymbol{u}_0)) + \mathcal{E}_f(\phi_0))
\end{aligned} \tag{45}
$$

for $n = 0, 1, 2, \cdots, N-1$. In (44) and (45), the energy for the structure is defined as,

$$
\mathcal{E}_s(\boldsymbol{u}^h) \quad = \quad \frac{1}{2}\,(\dot{\boldsymbol{u}}^h\,,\,\rho_s\dot{\boldsymbol{u}}^h)_{\Omega_s} + \frac{1}{2}\,a(\boldsymbol{u}^h\,,\,\boldsymbol{u}^h)_{\Omega_s} \tag{46}
$$

while the energy for the acoustic fluid has been defined previously in (40). Equation (45) indicates that *the proposed space-time formulation for structural acoustics is unconditionally stable.*

4 High-order Accurate Radiation Boundary Conditions

To obtain high-order accurate radiation boundary conditions we start in the frequency domain with the reduced wave equation (Helmholtz equation) in the exterior domain

Ω_∞ with harmonic time dependence $e^{-i\omega t}$, and $\omega > 0$. The boundary-value problem under consideration is,

$$\nabla^2\phi + k^2\phi = 0 \qquad \text{in } \Omega_\infty \tag{47}$$

$$\phi = \bar{\phi} \qquad \text{on } \Gamma_\infty \tag{48}$$

$$\lim_{r\to\infty} \sqrt{r}\left(\frac{\partial\phi}{\partial r} - ik\phi\right) = 0 \tag{49}$$

where $k = \omega/c \geq 0$ is the acoustic wavenumber and $\bar{\phi}$ is the restriction of ϕ to Γ_∞. Equation (49) is the Sommerfeld radiation condition for the two-dimensional problem. Restricting the artificial boundary Γ_∞ to be of separable geometry, in this case a circle of radius $r = R$ in two-dimensions, we are able to express the general solution to this problem as an infinite series of cylindrical wave harmonics:

$$\phi(r,\theta) = \sum_{n=0}^{\infty} H_n(kr)(a_n\cos n\theta + b_n \sin n\theta), \qquad r \geq R \tag{50}$$

where for outgoing waves, $H_n(kr)$ are cylindrical Hankel functions of the first kind of order n. The function $\bar{\phi}(\theta)$ in (48) can be expanded in a Fourier series in the circumferential coordinate θ, and after equating its Fourier coefficients with (50) evaluated at $r = R$, i.e. setting $\phi(R,\theta) = \bar{\phi}(\theta)$, we obtain,

$$\phi(r,\theta) = \sum_{n=0}^{\infty} \frac{H_n(kr)}{H_n(kR)}\alpha_n(\theta) \tag{51}$$

where

$$\alpha_n(\theta) = \frac{\varepsilon_n}{\pi}\int_0^{2\pi} \cos n(\theta-\theta')\ \phi(R,\theta')\ d\theta'$$

and $\varepsilon_0 = 1/2$ and $\varepsilon_n = 1, n \geq 1$.

Differentiating (51) with respect to r evaluated at $r = R$ results in the exact Dirchlet-to-Neumann (DtN) boundary condition in the frequency domain presented by Keller and Givoli [8].

$$\frac{\partial\phi}{\partial n}(R,\theta) = \int_0^{2\pi} s(\theta-\theta')\ \phi(R,\theta')\ R\ d\theta' \tag{52}$$

where

$$s(\theta-\theta') = \frac{\varepsilon_n\ k}{\pi R}\sum_{n=0}^{\infty}\frac{H_n'(kR)}{H_n(kR)}\cos n(\theta-\theta')$$

and $0 \leq \theta < 2\pi$ is the polar angle. Eq. (52) can be written in operator form as,

$$\frac{\partial\phi}{\partial n} \quad = \quad -\mathbb{S}\,\phi \qquad \text{on } \Gamma_\infty \tag{53}$$

which represents a relation between Dirichlet and Neumann data through the linear operator $\mathbb{S}$. The DtN map $\mathbb{S}$, represents the exact impedance for the exterior acoustic fluid restricted to the artificial boundary. Furthermore, the operator $\mathbb{S}$ is an integral operator coupling all points on the artificial boundary Γ_∞, resulting in a nonlocal boundary condition. The direct time-dependent counterpart to this condition involves a convolution integral over time. As a result of the time integral, the boundary condition is nonlocal in time, requiring the storage of a large pool of historical data for long time solutions. For an efficient algorithm, it is desirable to obtain a time-dependent counterpart to (52) which takes the form of a local boundary condition in both time and space.

4.1 Local Boundary Operators in the Frequency Domain

In the freqency domain, (Givoli and Keller [9]) have shown that it is possible to derive a sequence of spatially local (differential) operators which share the property of the DtN map (52); namely, the ability to exactly represent the first N cylindrical wave harmonics on a circular boundary Γ_∞. However, in two spatial dimensions, time-dependent counterparts with local temporal derivatives are not readily obtained do to the difficulty in obtaining an exact inverse Fourier transform for the two-dimensional Hankel function. To address this difficulty, high-order accurate boundary conditions which are local in both space and time are constructed by expressing the exact solution (51) in an alternative form, using an asymptotic approximation for $H_n(kr)$, and then following a procedure outlined in Bayliss and Turkel [10, 11] for annilating radial terms in the resulting expansion. To this end, a recurrence formula for Hankel functions is used to express $H_n(kr)$ in (51) as a linear combination of $H_0(kr)$ and $H_1(kr)$,

$$H_n(kr) = P_n H_0(kr) + Q_n H_1(kr) \tag{54}$$

where $P_n(1/kr)$ and $Q_n(1/kr)$ are Lommel's polynomials of degree n in the variable $1/kr$, Watson [15]. The resulting expression, namely:

$$\phi(r,\theta) = H_0(kr)\sum_{n=0}^{\infty} P_n \frac{\alpha_n(\theta)}{H_n(kR)} + H_1(kr)\sum_{n=0}^{\infty} Q_n \frac{\alpha_n(\theta)}{H_n(kR)} \tag{55}$$

can be rearranged to take the form of a series expansion in $1/kr$:

$$\phi(r,\theta) = H_0(kr)\sum_{j=0}^{\infty} \frac{F_j(\theta)}{(kr)^j} + H_1(kr)\sum_{j=0}^{\infty} \frac{G_j(\theta)}{(kr)^j} \tag{56}$$

This series is uniformly and absolutely convergent and can be differentiated termwise with respect to r any number of times, see Karp [16]. The coefficients $F_j(\theta)$ and $G_j(\theta)$

are nonlocal functions, and if evaluated explicitly would lead to an exact boundary condition coupling all points around the boundary Γ_∞. To eliminate this source of non-locality, the asymptotic expansion of cylindrical Hankel functions, for large kr, is used, see e.g. WATSON [15]:

$$H_n(kr) = (-i)^n \sqrt{\frac{2}{\pi kr}} e^{i(kr-\pi/4)} \left\{ 1 - \frac{(4n^2-1)}{8ikr} + \mathcal{O}\left((kr)^{-2}\right) \right\} \tag{57}$$

After substituting this approximation for $H_0(kr)$ and $H_1(kr)$ into (56) and accepting an error of the order $\mathcal{O}\left((kr)^{-3/2}\right)$ an approximate asymptotic expansion is obtained:

$$\phi(r,\theta) \sim \hat{\phi}(r,\theta) = \sqrt{\frac{2}{\pi kr}} e^{i(kr-\pi/4)} \sum_{j=0}^{\infty} \frac{f_j(\theta)}{(kr)^j} \tag{58}$$

Following the procedure outlined in BAYLISS AND TURKEL [10, 11], a sequence of local differential operators which eliminate the first m nonlocal terms $f_j(\theta)$ in this asymptotic expansion is found. Splitting the series (58) into two sums and multiplying by $r^{m-1/2}$ throughout gives,

$$r^{m-1/2}\hat{\phi} = e^{ikr} \sum_{j=1}^{m} r^{m-j} g_j(\theta) + e^{ikr} \sum_{j=m+1}^{\infty} r^{m-j} g_j(\theta) \tag{59}$$

where the coefficients are regrouped as,

$$g_j(\theta) = \sqrt{\frac{2}{\pi}} e^{-i\pi/4} f_{j-1}(\theta) k^{1/2-j}$$

Applying the local differential operator

$$L_o = \frac{\partial}{\partial r} - ik \tag{60}$$

to the power of m, i.e. $(L_o)^m$ to both sides of (59), the first sum is annihilated: For $m = 1$ and $m = 2$,

$$\begin{aligned} B_1\hat{\phi} &= L_o^1(r^{1/2}\hat{\phi})/r^{1/2} = (L_o + 1/2r)\hat{\phi} \\ B_2\hat{\phi} &= L_o^2(r^{3/2}\hat{\phi})/r^{3/2} = (L_o + 5/2r)(L_o + 1/2r)\hat{\phi} \end{aligned}$$

By analogy, the family of local operators of order m are obtained recursively as,

$$B_m = \prod_{j=1}^{m} \left(\frac{\partial}{\partial r} - ik + \frac{2j - 3/2}{r} \right) \tag{61}$$

The B_m operator matches the first m terms in the expansion (58) with a remainder of order,

$$B_m\hat{\phi} = \mathcal{O}\left(r^{-m}(kr)^{-m-1/2}\right) \tag{62}$$

For fixed kr and increasing m, then $\lim_{m\to\infty} B_m(\phi) = 0$. Thus the hierarchical family of approximate boundary conditions can be taken as,

$$B_m(\phi) := 0 \qquad \text{on} \ \ \Gamma_\infty \tag{63}$$

These are higher order boundary conditions on Γ_∞ and provide increasing accuracy with m, allowing in principle the computational region to be reduced to a minimum. Note that the accuracy of these local operators depends strongly on the parameter kr such that for a fixed r, i.e. $\lim_{k\to\infty} B_m(\phi) = 0$. In this way, these local operators can be viewed as high frequency approximations where as the frequency (wavenumber) is increased relative to the distance from the structure to the radiation boundary, the accuracy can be expected to increase (although not uniformly). On the other hand, the operators will be increasingly accurate as the position of the artificial boundary $r = R$, approaches infinity, i.e., $\lim_{r\to\infty} B_m(\phi) = 0$.

4.2 Local Boundary Operators in the Time Domain

Local time-dependent counterparts to (61) are obtained by applying an inverse Fourier transform, in effect replacing every occurrence of the operator $-ik$ by $\frac{1}{c}\frac{\partial}{\partial t}$ with the result,

$$B_m = \prod_{j=1}^{m} \left(\frac{\partial}{\partial r} + \frac{1}{c}\frac{\partial}{\partial t} + \frac{2j - 3/2}{r} \right) \tag{64}$$

The space-time finite element method provides a natural variational setting for the incorporation of the time-dependent radiation boundary conditions, where the temporal derivatives appearing in the boundary operator may be approximated within a space-time slab using standard C^0 continuous shape functions in time. A direct approach in which to implement (64) is to eliminate the high-order radial derivatives in favor of tangential and temporal derivatives through recursive use of the wave equation. It is then possible to define the operators $\mathbb{S}_m$ in (7) as,

$$B_m(\phi) \equiv \frac{\partial \phi}{\partial n} + \mathbb{S}_m\, \phi \qquad \text{on} \ \ \Gamma_\infty \tag{65}$$

which implies

$$\nabla\phi \cdot \boldsymbol{n} \quad = \quad -\mathbb{S}_m\, \phi \qquad \text{on} \ \ \Gamma_\infty \tag{66}$$

which is in the form of a local, (i.e. differential) Dirichlet to Neumann boundary condition through the linear map $\mathbb{S}_m$. Using this approach, the first two operators $\mathbb{S}_m$ for m equal to 1 and 2 are:

$$\mathbb{S}_1\, \phi \quad = \quad \frac{1}{2R}\phi + \frac{1}{c}\dot{\phi} \tag{67}$$

$$\mathbb{S}_2\, \phi \quad = \quad \frac{1}{2R}(3/4 - \frac{\partial^2}{\partial\theta^2})\phi + \frac{3}{2c}\dot{\phi} + \frac{R}{c}\frac{\partial\dot{\phi}}{\partial r} + \frac{R}{c^2}\ddot{\phi} \tag{68}$$

These local boundary conditions are incorporated into the space-time finite element method as natural boundary conditions, i.e., they are enforced weakly in space-time. The first-order operator $\mathbb{S}_1$ is equivalent to the cylindrical damper described earlier in (12) and is implemented in the variational equation (21) through the operators (24) and (28). For $\mathbb{S}_2$, the space-time operator on the truncation boundary generalizes to,

$$\begin{aligned} E_r(w^h\,,\,\phi^h)_n &= \frac{3}{8R}(\dot{w}^h\,,\,\phi^h)_{(\Upsilon_\infty)_n} + \frac{1}{2R}(\dot{w}^h_{,\theta}\,,\,\phi^h_{,\theta})_{(\Upsilon_\infty)_n} \\ &+ \frac{3}{2c}(\dot{w}^h\,,\,\dot{\phi}^h)_{(\Upsilon_\infty)_n} + \frac{R}{c}(\dot{w}^h\,,\,\dot{\phi}^h_{,r})_{(\Upsilon_\infty)_n} \\ &+ \frac{R}{c^2}(\dot{w}^h\,,\,\ddot{\phi}^h)_{(\Upsilon_\infty)_n} \\ &+ \frac{3}{8R}(w^h(t_n^+)\,,\,\phi^h(t_n^+))_{\Gamma_\infty} \\ &+ \frac{1}{2R}(w^h_{,\theta}(t_n^+)\,,\,\phi^h_{,\theta}(t_n^+))_{\Gamma_\infty} \\ &+ \frac{R}{c^2}(\dot{w}^h(t_n^+)\,,\,\dot{\phi}^h(t_n^+))_{\Gamma_\infty} \end{aligned} \tag{69}$$

In the second and seventh term in (69), continuity requirements due to second-order tangential derivatives $\partial^2/\partial\theta^2$, are relaxed on the artificial boundary Γ_∞, by use of the identity,

$$(w\,,\,\phi_{,\theta\theta})_{\Gamma_\infty} = -(w_{,\theta}\,,\,\phi_{,\theta})_{\Gamma_\infty} \tag{70}$$

Information from the previous space-time slab on Γ_∞ is incorporated consistently through temporal jump terms. For $\mathbb{S}_2$, information from the previous slab $\phi^h(\boldsymbol{x}, t_n^-)$ for $\boldsymbol{x}$ on Γ_∞ is incorporated as,

$$\begin{aligned} L_r(w^h)_n &= \frac{3}{8R}(w^h(t_n^+)\,,\,\phi^h(t_n^-))_{\Gamma_\infty} \\ &+ \frac{1}{2R}(w^h_{,\theta}(t_n^+)\,,\,\phi^h_{,\theta}(t_n^-))_{\Gamma_\infty} \\ &+ \frac{R}{c^2}(\dot{w}^h(t_n^+)\,,\,\dot{\phi}^h(t_n^-)_{\Gamma_\infty} \end{aligned} \tag{71}$$

Temporal continuity is weakly enforced across space-time slabs on Γ_∞ through the combination of the loading operator (71) and the last three operators in (69).

Because the time-discontinuous formulation allows for the use of $C^0(I_n)$ interpolations in time to represent the high-order time derivatives, it is possible to implement the boundary conditions in the sequence (64) up to any order desired. However for operators extending beyond $m > 3$, the lowest possible order of spatial continuity

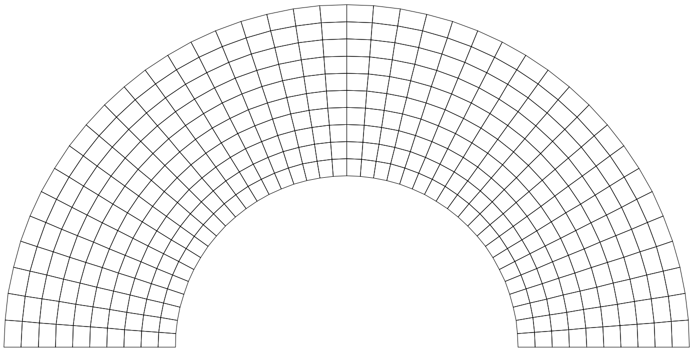

Fig. 3. Computational domain bounded internally by a radiating circular cylinder of radius a, and bounded externally by a circular artificial truncation boundary of radius $R = 2a$. By symmetry, only the upper half is discretized with 400 elements.

on Γ_∞ that can be achieved after integration by parts is $C^1(\Gamma_\infty)$. For these high-order operators a layer of boundary elements adjacent to Γ_∞, possessing high-order tangential continuity on Γ_∞ are needed.

5 Numerical Examples

In this section numerical simulations of transient radiation and scattering are performed in order to demonstrate the effectiveness of the time-discontinuous Galerkin space-time finite element method to model two-dimensional wave phenomena. The problems studied are primarily designed to assess the performance of the two-dimensional, local time-dependent radiation boundary conditions when implemented in the space-time formulation. To clarify the analysis, the structure is assumed rigid so that the computational domain simplifies to the fluid region only. Standard isoparametric space-time elements with C^0 quadratic shape functions in both space and time dimensions are used for all the numerical examples presented.

5.1 Circumferential harmonic radiation

In this example we study the problem of an infinite circular cylinder of radius $a = 1$, with circumferentially harmonic radiation loading,

$$\phi(a, \theta, t) = \cos n\theta \sin \omega t \qquad \text{for } 0 \leq \theta < 2\pi\,, \quad t > 0 \tag{72}$$

The exact steady-state solution for this problem is for $r \geq a$,

$$\phi(r,\theta,t) = -\mathrm{Imag}\left\{ \frac{H_n(kr)}{H_n(ka)} \cos n\theta \mathrm{e}^{-i\omega t} \right\} \tag{73}$$

This example is used to quantify the accuracy of the sequence of local time-dependent radiation boundary conditions $\mathbb{S}_m$ in a controlled setting. To obtain a challenging test problem we take the artificial boundary Γ_∞ to be a circular boundary of radius $R = 2a$ as illustrated in Figure 3, and increase the radiation loading from $n = 1$ to $n = 2$. As the wave harmonic n is increased the radiation pattern becomes increasingly complex, and this problem becomes more difficult to solve. It is expected that the higher-order operators in the sequence $\mathbb{S}_m$, $m = 1, 2, \cdots$ will be increasingly accurate compared to the simple *PW* damper, denoted by $\mathbb{S}_0$ and defined in (11).

Using symmetry, the computational domain is taken as, $\Omega = \{a < r < R,\ 0 \leq \theta < \pi\}$, and Ω is discretized with 10 elements in the radial direction, and 40 elements in the polar direction; see Figure 3. A time-harmonic solution is obtained by starting from rest with zero initial conditions on ϕ and $\dot{\phi}$ and driving the solution to steady-state with a uniform time increment of $\Delta t = 0.1$.

Figure 4 illustrates the contours of the space-time finite element solution for the radiation loading (72) with $n = 1$ and a driving frequency of $ka = \omega a/c = 1$. Results are compared for the solution incorporating the simple 'plane-wave' boundary operator $\mathbb{S}_0$, the first-order operator $\mathbb{S}_1$, and the second-order operator $\mathbb{S}_2$. The solution sample time of $t = 30$ is chosen such that many spurious reflections between the artificial boundary and the radiating cylinder could have occurred. Figure 5(top) shows the profile of the solution plotted around the circular artificial boundary while Figure 5(bottom) shows the solution plotted along a radial line located at the angle $\theta = 0$. The results show that for this frequency and location of the radiation boundary, the low-order boundary conditions $\mathbb{S}_0$ and $\mathbb{S}_1$ display significant errors in the solution, while the second-order boundary condition $\mathbb{S}_2$ gives a remarkably accurate solution.

As the harmonic loading is increased to $n = 2$, the acoustic radiation pattern becomes more complex. For a driving frequency $ka = 1$, significant errors occur in the solution using $\mathbb{S}_0$ or $\mathbb{S}_1$, while the solution using $\mathbb{S}_2$ remains accurate throughout the computational domain, see Figures 6 and 7. Further results for harmonics of order $n = 3, 4, 5$ and increasing kR are reported in [6]. The numerical results confirm the estimate given in (62), that as the frequency is increased the accuracy of the local radiation boundary conditions increases, while the operator $\mathbb{S}_2$ outperforms the lower order operators $\mathbb{S}_1$ and $\mathbb{S}_0$ as expected.

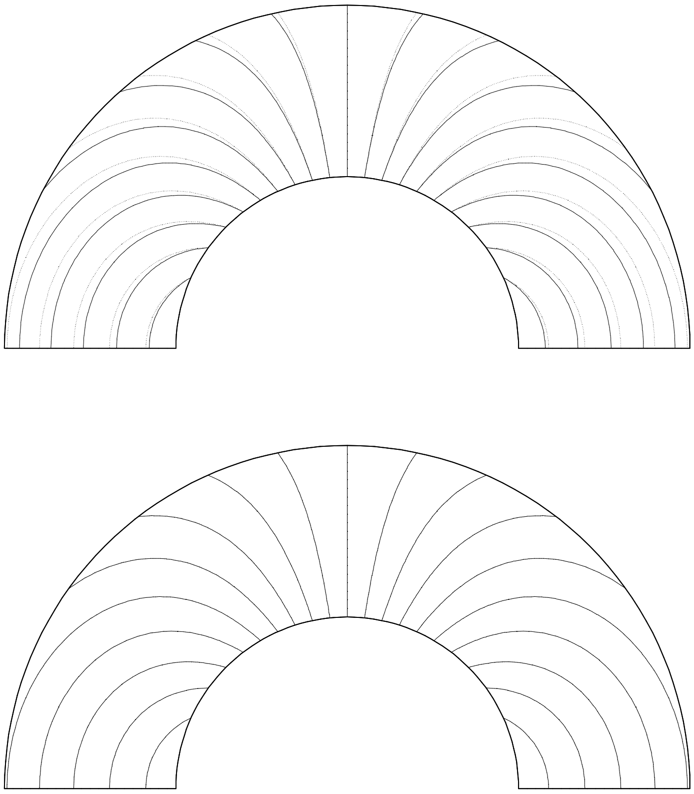

Fig. 4. Radiation from a circular cylinder with circumferential harmonic $n = 1$, and normalized frequency $ka = 1$. Contours of space-time solution at time $t = 30$, using local boundary conditions, (Top): first-order S_1, (Bottom): second-order S_2. Dotted contours denote analytical solution. Scale: (Max/Min $\pm$ 0.988)

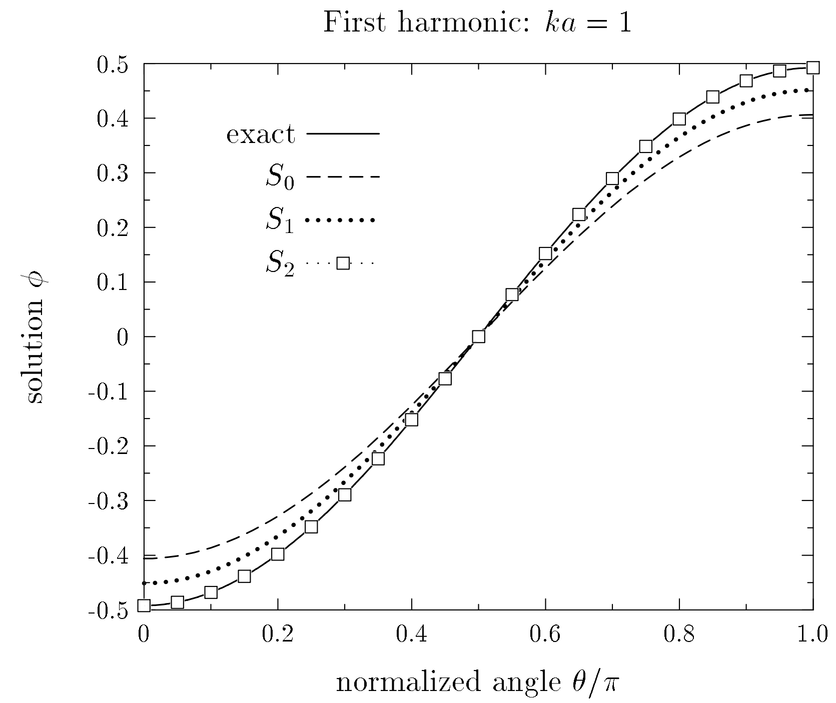

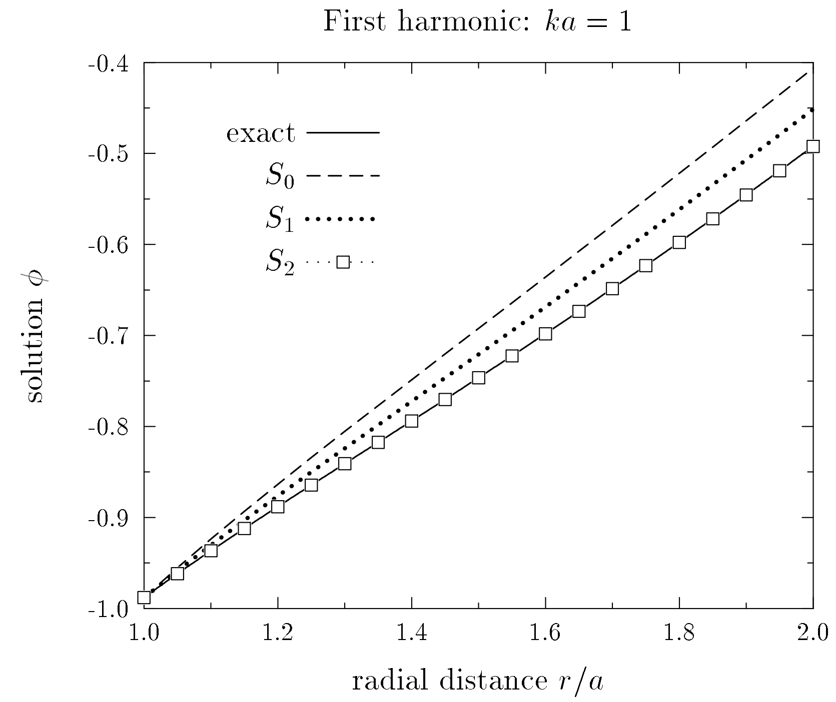

Fig. 5. Circumferential wave harmonic $n = 1$: Results at $t = 30$, comparing the 'plane-wave' S_0, first-order S_1, and second-order S_2 boundary conditions. (Top): Solution profile on the artificial boundary $r = R$. (Bottom): Solution plotted along radial line at $\theta = 0$.

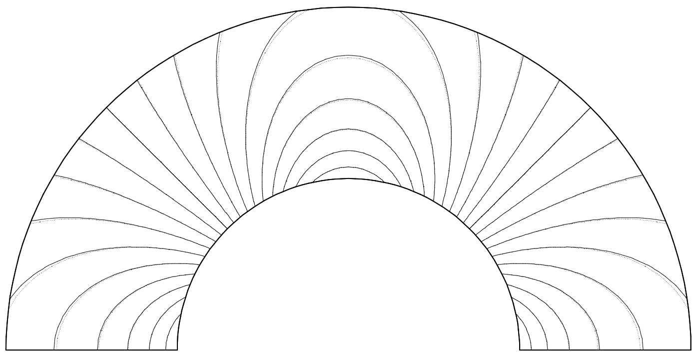

Fig. 6. Radiation from a circular cylinder with circumferential harmonic $n = 2$, and normalized frequency $ka = 1$. Contours of space-time solution at time $t = 30$, using the second-order S_2 local boundary condition. Dotted contours denote analytical solution. Scale: (Max/Min $\pm$ 0.988)

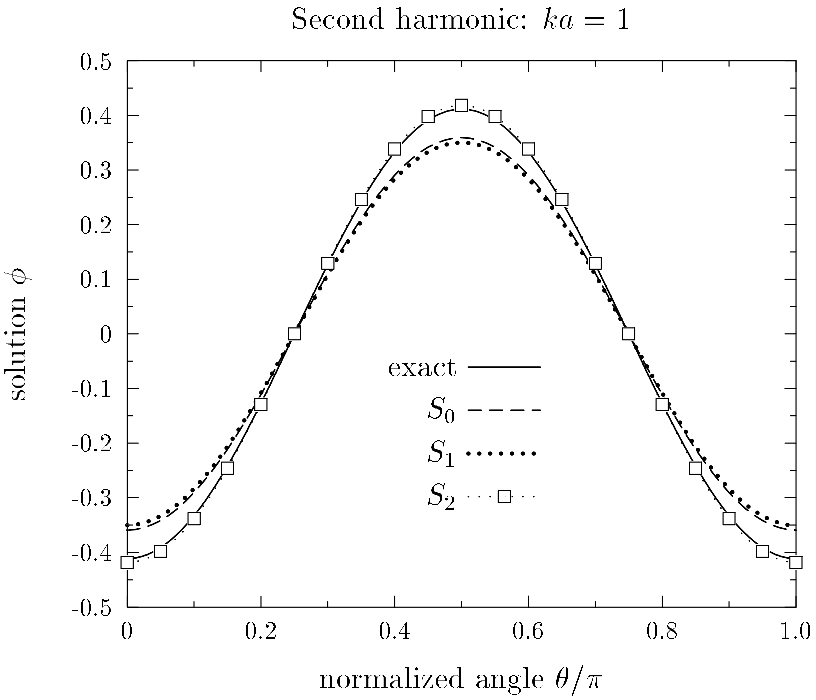

Fig. 7. Circumferential wave harmonic $n = 2$: Results at $t = 30$, comparing the 'plane-wave' S_0, first-order S_1, and second-order S_2 boundary conditions. Solution profile on the artificial boundary $r = R$.

5.2 Radiation from a line element on a cylinder

To study the accuracy of the local radiation boundary conditions for a problem involving an infinite number of circumferential harmonics, we consider the non-uniform radiation from a line element on an infinite circular cylinder of radius $r = a$, with loading

$$\phi(a, \theta, t) = \sin \omega t, \qquad \text{for } -\theta_p \leq \theta \leq \theta_p, \quad t > 0 \tag{74}$$

Elsewhere on the surface $r = a$, a homogeneous condition is prescribed. The steady-state analytical solution for this problem is,

$$\phi(r, \theta, t) = -\text{Imag}\left\{ \sum_{n=0}^{\infty} \frac{H_n(kr)}{H_n(ka)} \left[\frac{\epsilon_n \sin \theta_p}{n\pi} \right] \cos n\theta \, \mathrm{e}^{-i\omega t} \right\} \tag{75}$$

where $\epsilon_0 = 1/2$ and $\epsilon_n = 1, n \geq 1$. For low values of the normalized wavenumber ka, this solution is relatively uniform in the circumferential direction. The directionality of the solution grows as the wavenumber k is increased, and the solution becomes attenuated at the side of the cylinder opposite the radiating element.

In this example, the properties and discretization are unchanged from the previous problem. Figure 8 shows the contours of the solution for $ka = 3$. Results are compared to the analytical series solution nodally interpolated with the mesh employed. The low-amplitude oscillations in the vicinity of the inner boundary for the analytical solution are a result of the difficulty the series solution has in resolving the discontinuity in the loading at $\theta_p = 13.5^o$, and are not relevant to the validation of the numerical results. Near $\theta = 0$, solutions using either the boundary condition $\mathbb{S}_1$ or $\mathbb{S}_2$ accurately capture the physics of the problem while as the wave spreads to the back-side of the cylinder at $\theta = 180^o$, the solution using $\mathbb{S}_1$ deteriorates significantly while $\mathbb{S}_2$ maintains an accurate solution in this difficult region. These results are quantified in Figure 9, as a profile of the solution on Γ_∞ at $r = R$. Results from this example illustrate the significant improvement in the numerical solution using the second-order operators $\mathbb{S}_2$, in comparison to the numerical solution using the operators $\mathbb{S}_1$ or $\mathbb{S}_0$, for problems involving an infinite number of spatial harmonics.

5.3 Transient scattering from a circular cylinder

To study a problem involving scattering, we consider the infinite circular cylinder of radius $r = a$, now with an incident pulse reflecting off the wet surface. In the upper left corner of Figure 10 the finite element spatial discretization of the computational domain $\Omega = \{a \leq r \leq R, \, 0 \leq \theta \leq 2\pi\}$ bounded internally by the projection of the infinite circular cylinder, and externally by a circular artificial boundary with

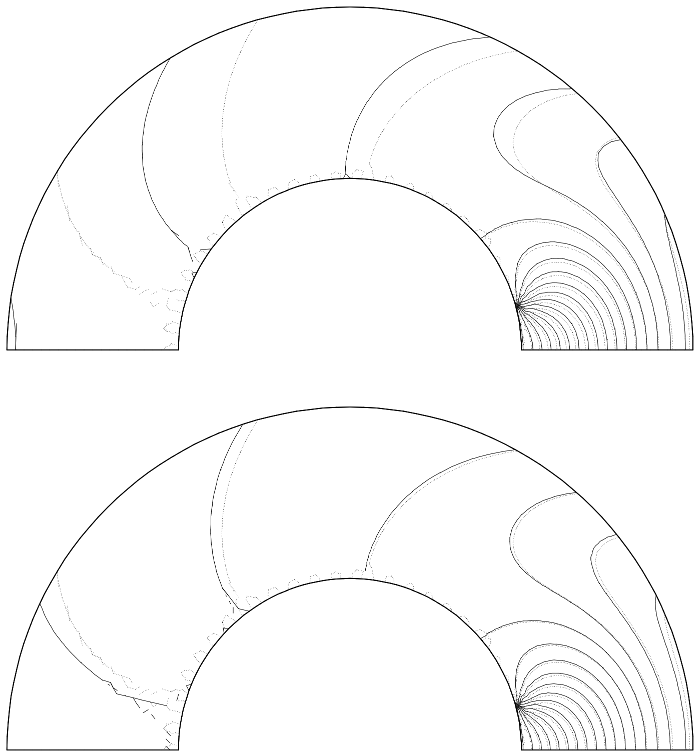

Fig. 8. Solution contours for radiating element on a circular cylinder: Results at time $t = 30$ and normalized frequency $ka = 3$. Space-time solution with local boundary condition, (Top): $\mathbb{S}_1$ (Bottom): $\mathbb{S}_2$ Dotted contours denote analytic series solution (50 terms). Scale: (Max 0.254, Min -0.988)

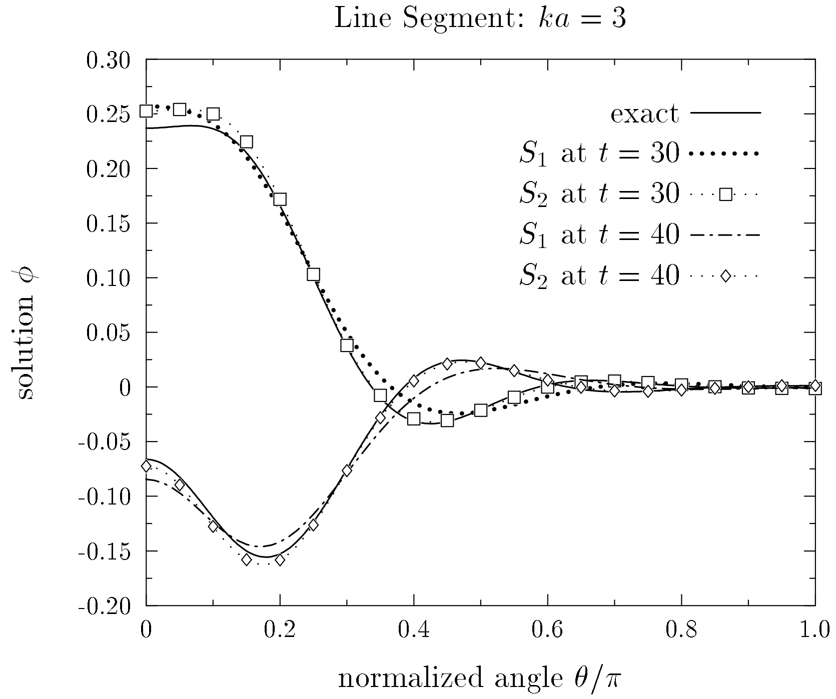

Fig. 9. Radiating circular cylinder with line segment loading. Solution profile on the artificial boundary $r = R$.

radius $R = 3a$ is shown. By symmetry only half the problem is modeled with 1200 quadratic elements. An incident pulse of short duration is generated by an acoustic source positioned midway between the cylinder and the circular artificial boundary, Γ_∞. This example represents a challenging problem where both the incident wave pulse and scattered waves should be transmitted through Γ_∞ with negligible reflection.

For this two-dimensional problem, the second-order local boundary condition $\mathbb{S}_2$ defined in (68) is prescribed on Γ_∞. The source $f = \delta(x_0, y_0) \sin \omega t$ and $t \in [0\,,\, 0.5]$, is positioned inside the computational domain at $(x_0, y_0) = (2a, 0)$. Setting the phase speed at $c = 1$ and frequency $\omega = 2\pi$ results in a challenging initial condition. The numerical simulation is continued until just prior to reaching the practical disappearance of the signal from the computational domain.

The numerical simulation at the end of the initial pulse is shown in Figure 10 at $t = 0.5$. The subsequent figures show the contours of the scattering phenomena with homogeneous Dirichlet boundary conditions on the cylinder surface $r = a$, i.e. 'release' boundary conditions. The following sequence of events occur: At $t = 1.5$ the incident pulse has expanded in a cylindrical wave and has just begun to reflect off the surface of the inner cylinder, while at the artificial boundary, the wave front passes through the boundary with no observable reflection. At $t = 2.5$ the incident wave continuous to diffract around the cylinder, creating a backscattered cylindrical wave that moves to the right and passes through the wake of the incident wave. At $t = 3.0$ the backscattered wave has just reached the artificial boundary. At $t = 4.0$ the backscattered wave is also transmitted through the artificial boundary with no observable reflection. As a result of the homogeneous Dirichlet boundary conditions, the contours near the wet surface lie parallel to the cylinder outline and the amplitude of the backscattered wave is negative.

Figure 11(left) shows the transient solution on the artificial boundary at the point $(r\,,\,\theta) = (R\,,\,0)$. Prior to time $t = 1$, the initial pulse has not reached the boundary Γ_∞ as indicated by the quiescent solution. Upon arrival at time $t = 1$, the solution advances as a sharp pulse with a wake of decaying amplitude. At time $t = 2.5$, the backscattered wave reaches Γ_∞, as indicated by the pulse of negative amplitude. For comparison, Figure 11(right) shows the transient solution when the boundary condition at the inner cylinder is changed to a homogeneous Neumann condition, i.e. a 'rigid' boundary condition. In this case the backscattered wave takes a positive amplitude.

5.4 Transient scattering from a cylinder with tapered ends

As a final example of engineering significance, consider the time-dependent scattering from a rigid infinite cylinder with conical-to-spherical ends and a large length to width ratio, $L/d = 6.1$. Figure 12 illustrates the finite element spatial discretization of the computational domain. A total of 1600 quadratic elements are used and the second-order local boundary condition $\mathbb{S}_2$ defined in (68) is prescribed on Γ_∞.

For this problem, the source $f = \delta(x_0, y_0)\sin\omega t$ with time interval $t \in [0, 3]$, is positioned inside the computational domain simulating an oblique incident wave. The phase speed is set at $c = 1$ with frequency $\omega = \pi/3$. Homogeneous Dirichlet boundary conditions are prescribed on the cylinder wet surface. This example represents a challenging problem where the multiple-scales involving the ratio of the wavelength to diameter and length dimension play a critical role in the complexity of the resulting scattered wave field.

The numerical simulation at the end of the initial pulse at $t = 3$ is shown at the top of Figure 13. The subsequent illustrations in Figure 13 show the contours of the scattering phenomena as time progresses. At $t = 6$ the incident pulse has expanded in a cylindrical wave and has just reached the boundary of the cylinder, while at the artificial boundary, the wave front passes through with negligible reflection. At $t = 9$ through $t = 12$, the incident wave has begun to reflect off the 'release' boundary, creating a complicated backscattered wave. As a result of homogeneous Dirichlet boundary conditions, the amplitude of the backscattered wave is negative. At $t = 15$,

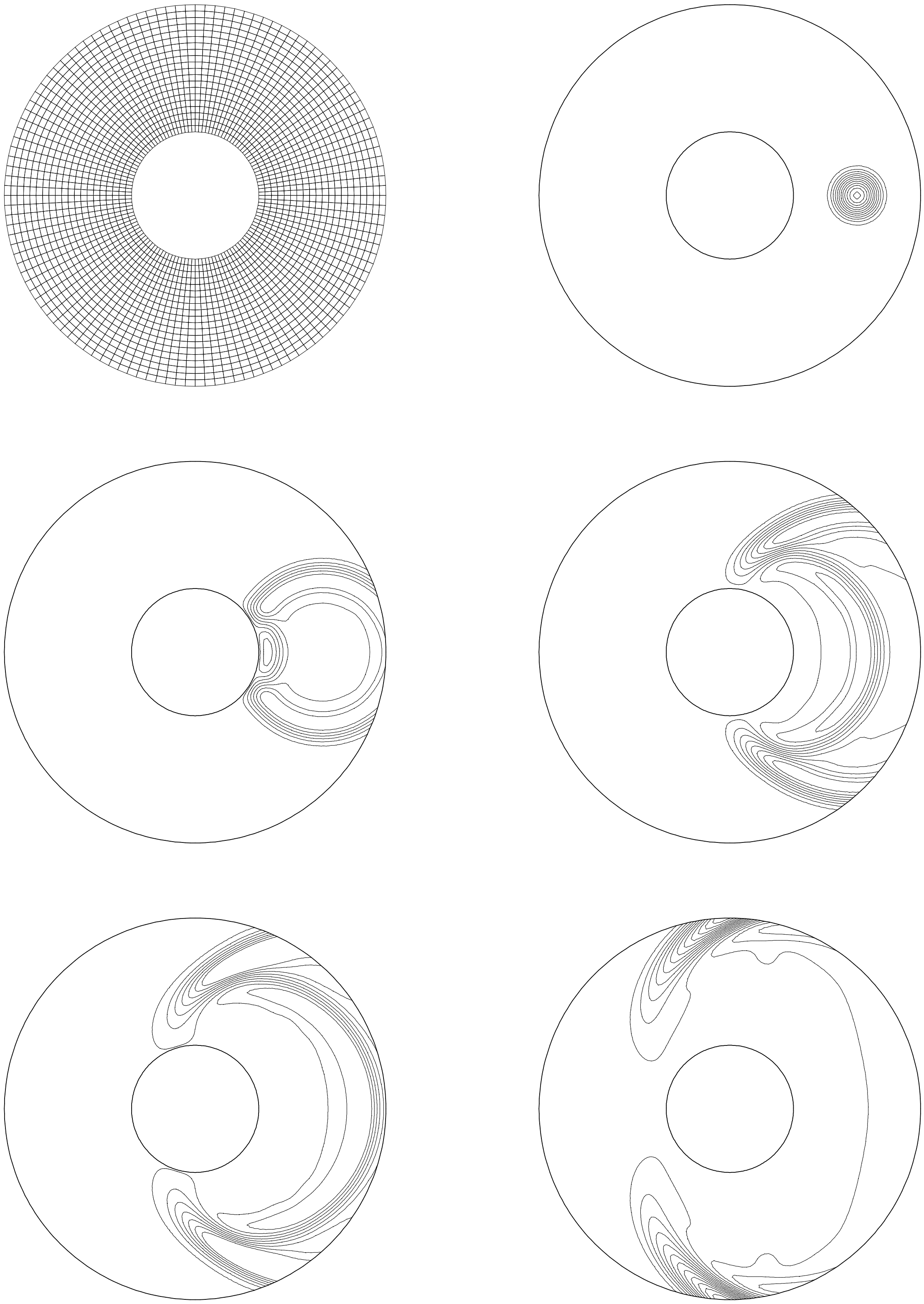

Fig. 10. Scattering from an infinite 'release' circular cylinder due to point source. Solution contours shown at the end of the initial pulse at $t = 0.5$ and later times $t = 1.5$, $t = 2.5$, $t = 3$, and $t = 4$.

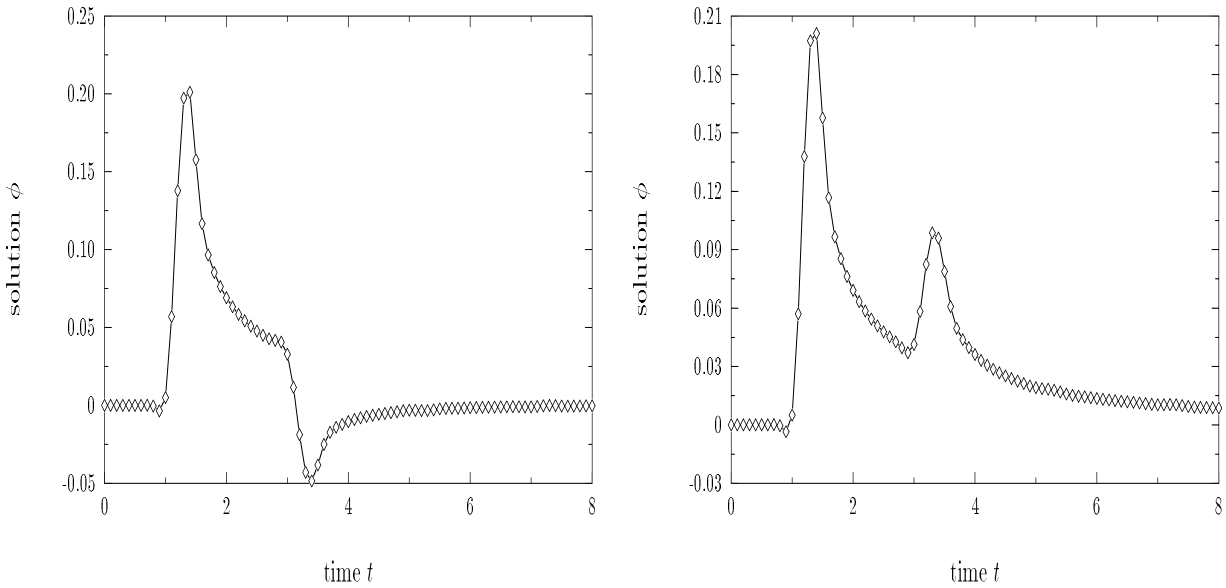

Fig. 11. Scattering from an infinite circular cylinder: Solution time-history on the artificial boundary Γ_∞, at $\theta = 0$. (left) 'release' cylinder. (right) 'rigid' cylinder.

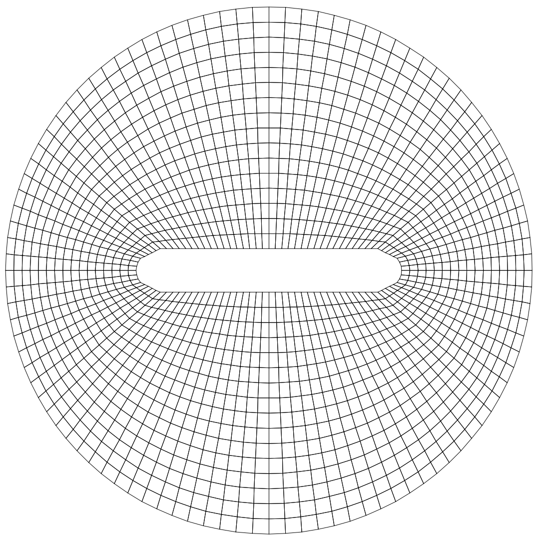

Fig. 12. Spatial discretization for cylinder with conical to spherical ends. (1600 quadratic elements)

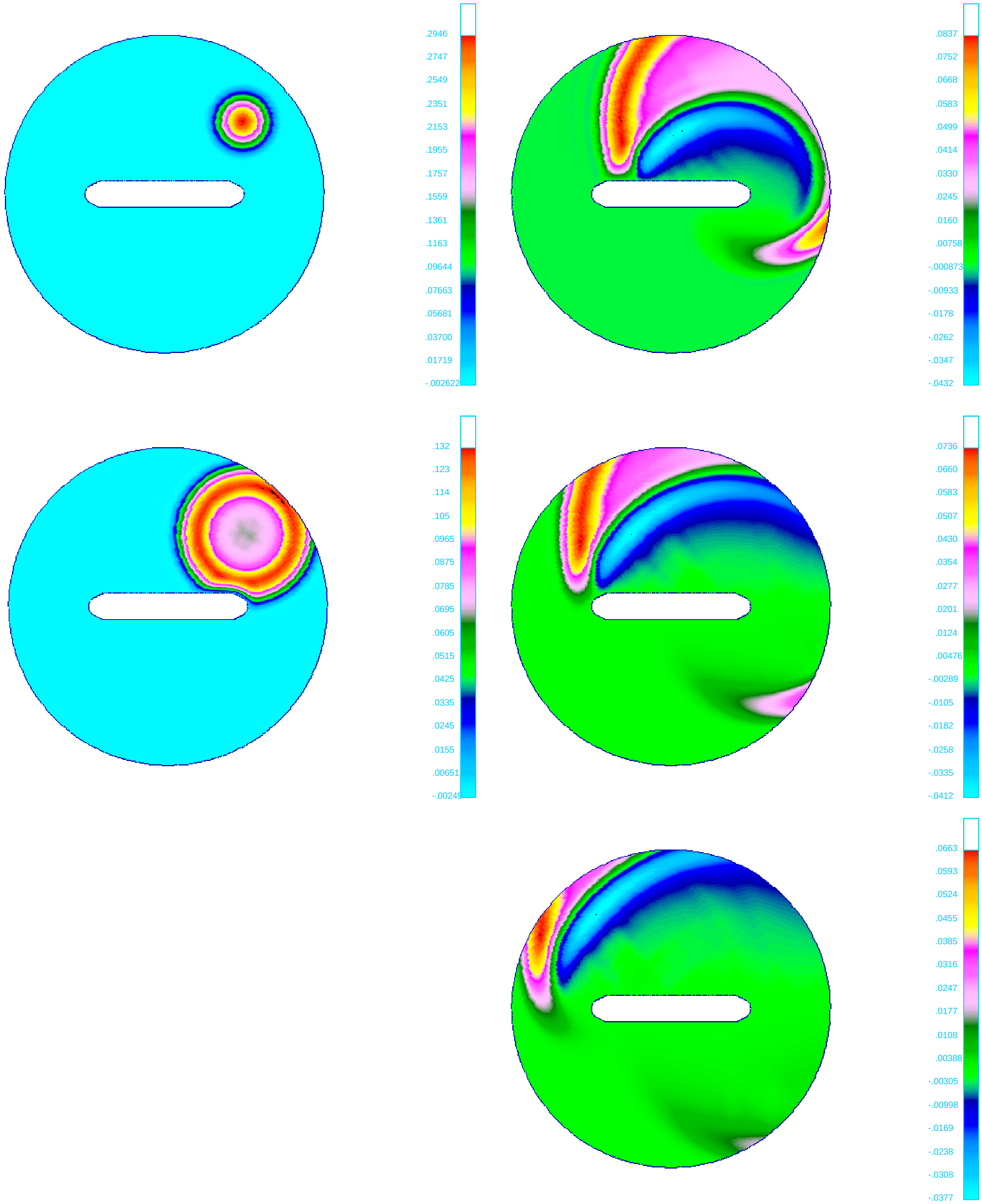

Fig. 13. Scattering from a 'release' cylinder with tapered ends due to a time-dependent point source. Solution contours shown at the end of the initial pulse at $t = 3$ and later times $t = 6, 12, 15, 18$.

the incident wave begins to scatter into a part that travels along the upper part of the cylinder, and a part that diffracts around the backside. The backscattered wave is seen to transmit through the radiation boundary with no observable reflection. At $t = 18$, the incident wave has passed over the cylinder and continues to be absorbed through the non-reflecting boundary. A quiescent state near the right of the cylinder suggests the effectiveness of the local boundary condition in absorbing outgoing waves.

6 Conclusions

For wave propagation in two dimensions, it is not possible to obtain local (differential) time-dependent radiation boundary conditions that exactly represent cylindrical wave harmonics. The difficulty can be traced to the representation of cylindrical Hankel functions appearing in the impedance coefficients of the exact Dirichlet-to-Neumann (DtN) map in the frequency domain. Because of this difficulty, we resort to an approximation to the exact solution for outgoing waves expressed as an asymptotic expansion for large frequency (short wavelength), normalized with the radius of the circular DtN boundary. Following the procedure outlined in Bayliss and Turkel [10, 11], a sequence of differential operators are defined which match the leading terms of the asymptotic approximation to provide local boundary conditions which are of progressively higher order and increasing accuracy. These boundary operators have an inverse Fourier transform allowing a family of boundary conditions that are local in space and time. After eliminating higher-order radial derivatives through the use of the second-order scalar wave equation, the sequence of non-reflecting boundary conditions can be incorporated into the time-discontinuous space-time variational equations as natural boundary conditions in a straightforward manner. Crucial to the unconditional stability of the formulation and positive form of the resulting matrix equations is the introduction of consistent temporal jump operators across space-time slabs restricted to the radiation boundary. The specific form of these operators are designed such that continuity of the solution across slabs is weakly enforced in a form consistent with the time-dependent radiation boundary conditions.

Numerical solutions for some carefully designed canonical acoustic radiation and scattering problems demonstrated the accuracy of the two-dimensional non-reflecting boundary conditions when implemented in the space-time finite element method. In particular, the effects of increasing cylindrical harmonics n, frequency $\omega = kc$, and the position of the fluid truncation boundary R, on the accuracy of the space-time finite element solution using the local radiation boundary operators was investigated. Results from this study are summarized in the following: (i) The local time-dependent boundary operators provide increasing accuracy with the order m used in the sequence; (ii) The accuracy depends strongly on the normalized frequency ka, in that the local operators can accurately capture increased wave harmonics as the frequency (wavenumber) is increased relative to the dimension of the radiator/scatterer; (iii) The operators are increasingly accurate as the position R of the artificial boundary is moved further away from the radiator/scatterer.

Numerical results confirmed the superiority of the second-order local non-reflecting boundary condition $\mathbb{S}_2$, in comparison to the first-order $\mathbb{S}_1$, and simple 'plane-wave' $\mathbb{S}_0$, operators. The examples also demonstrate that with proper consideration given to the position of the radiating boundary and frequency content of the time-dependent solution, the second-order boundary condition $\mathbb{S}_2$ is sufficiently accurate to capture the important physics associated with a variety of complicated transient scattering problems. While the numerical simulations have been limited to two-dimensional boundary conditions up to second-order, the time-discontinuous space-time finite element formulation is applicable to third and higher-order boundary conditions. It remains to be seen what (if any) additional advantage in terms of accuracy and economy can be achieved by the implementation of the third-order operators in the space-time formulation for structural acoustics.

References

[1] Hughes,T.J.R.; Hulbert,G.M. (1988): Space-time finite element methods for elastodynamics: Formulations and error estimates. *Comp. Meth. in Appl. Mech. Eng.* 66, 339-363.

[2] Givoli,D. (1991): Non-reflecting boundary conditions: A review. *J. Comput. Phys.*, 94, 1-29.

[3] Abboud,N.N. (1990): A Mixed finite element formulation for the transient and harmonic exterior fluid-structure interaction problem. *Ph.D. Dissertation, Stanford University*, Stanford, California, August 1990.

[4] Thompson,L.L.; Pinsky,P.M. (1993): New space-time finite element methods for fluid-structure interaction in exterior domains. in *Computational Methods for Fluid/Structure Interaction*, AMD-Vol. 178, ASME 1993, pp. 101-120.

[5] Thompson,L.L.; Pinsky,P.M. (1995): A Space-time finite element method for structural acoustics in infinite domains, Part I: Formulation, Stability, and Convergence. Accepted: *Comp. Meth. in Appl. Mech. Eng.*

[6] Thompson,L.L.: (1994): Design and analysis of space-time and Galerkin/least-squares finite element methods for fluid-structure interaction in exterior domains. *Ph.D. Dissertation, Stanford University*, Stanford, California, April 1994.

[7] Thompson,L.L.; Pinsky,P.M. (1995): A Space-time finite element method for structural acoustics in infinite domains, Part II: Exact time-dependent non-reflecting boundary conditions. Accepted: *Comp. Meth. in Appl. Mech. Eng.*

[8] Keller,J.B.; Givoli,D. (1989): Exact non-reflecting boundary conditions. *J. Comp. Phys.* 82, 172-192.

[9] Givoli,D.; Keller,J.B. (1990): Non-reflecting boundary conditions for elastic waves. *Wave Motion*, 12, 261-279.

[10] Bayliss, A.; Turkel, E. (1980): Radiation boundary conditions for wave-like equations. *Commun. Pure Appl. Math.*, 33, 707-725.

[11] Bayliss, A.; Gunzburger, M.; Turkel, E. (1982): Boundary conditions for the numerical solution of elliptic equations in exterior regions, *SIAM J. Appl. Math.* 42, 430-451.

[12] Pinsky,P.M.; Thompson,L.L. (1991): Accuracy of local non-reflecting boundary conditions for time-dependent structural acoustics. *Structural Acoustics*, NCA-Vol.12/AMD-Vol.128, 153-160.

[13] Pinsky,P.M.; Thompson,L.L.; Abboud,N.N. (1992): Local high order radiation boundary conditions for the two-dimensional time-dependent structural acoustics problem. *J. Acoust. Soc. Am.*, 91, 1320-1335.

[14] Hughes,T.J.R.; Franca,L.P.; Hulbert,G.M. (1989): A new finite element formulation for computational fluid dynamics: VIII. The Galerkin least squares method for advective-diffusive equations. *Comp. Meth. in Appl. Mech. Eng.* 73, 173-189.

[15] Watson,G.N. (1966): Theory of Bessel Functions, Cambridge U.P., Cambridge.

[16] Karp, S.N. (1961): A convergent far field expansion for two-dimensional radiation functions. *Commun. Pure Appl. Math.* XIV, 427-434.